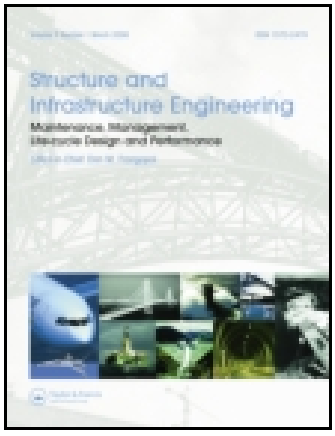

Structure and Infrastructure Engineering: Maintenance, Management, Life-Cycle Design and Performance

Publication details, including instructions for authors and subscription information:
http://www.tandfonline.com/loi/nsie20

Seismic performance of pile-founded fixed jacket platforms with chevron braces

Mohamed Nour El-Din[a] & Jinkoo Kim[b]

[a] Samsung Engineering Co Ltd, Seoul, Republic of Korea

[b] Department of Civil and Architectural Engineering, Sungkyunkwan University, Suwon, Republic of Korea

Published online: 12 May 2014.

To cite this article: Mohamed Nour El-Din & Jinkoo Kim (2015) Seismic performance of pile-founded fixed jacket platforms with chevron braces, Structure and Infrastructure Engineering: Maintenance, Management, Life-Cycle Design and Performance, 11:6, 776-795, DOI: 10.1080/15732479.2014.910536

To link to this article: http://dx.doi.org/10.1080/15732479.2014.910536

Structure and Infrastructure Engineering, 2015
Vol. 11, No. 6, 776–795, http://dx.doi.org/10.1080/15732479.2014.910536

Seismic performance of pile-founded fixed jacket platforms with chevron braces

Mohamed Nour El-Din[a1] and Jinkoo Kim[b]*

[a]*Samsung Engineering Co Ltd, Seoul, Republic of Korea;* [b]*Department of Civil and Architectural Engineering, Sungkyunkwan University, Suwon, Republic of Korea*

(*Received 23 September 2013; final version received 25 January 2014; accepted 31 January 2014; published online 12 May 2014*)

In this study, pile-founded jacket offshore structures with buckling-restrained braces (BRB) and conventional braces were designed using different methodologies such as performance-based (plastic design and displacement-based design) and strength-based (code procedure) methods, and their seismic performances for strength- and ductility-level earthquakes were compared. An analysis model of the jacket considering soil–pile structure interaction (SPSI) was developed by substituting the soil layers with equivalent nonlinear springs having pile–soil interaction characteristics. According to nonlinear static and dynamic analysis results, the application of BRB in chevron-braced jacket structures was found to enhance the seismic behaviour under ductility-level earthquakes. However, under strength-level earthquake, for which model structures mostly remained elastic, the enhancement was marginal. Among the different BRB design methods introduced, displacement-based design method produced more uniform plastic hinge distribution, while other methods provided better results in terms of maximum drift ratios. Based on the relative stiffness index and soil condition introduced in this study, it was found that for system with large ductility, simplified SPSI modelling could be used to reduce the computational cost especially for the preliminary design stage.

Keywords: seismic design; buckling restrained braces; fixed jacket offshore structures

1. Introduction

Fixed Steel Jacket Offshore Platforms (FSJOPs) have been extensively used to support offshore platforms in different locations of the world (Rodrigues & Jacob, 2005). Ensuring the integrity of offshore structures in high seismic areas is an essential requirement during design and maintenance phases. Previous research on FSJOBs generally focused on wave and current-induced responses, and research on inelastic seismic performance is relatively rare. This may be attributed to the fact that the design of offshore structure often controlled by other environmental loads such as wave, current and wind. American Petroleum Institute gives specific guidelines for configuring the structure and for proportioning the members to ensure the necessary ductility. It also requires that two different seismic ground motion levels should be checked, which are strength- and ductility-level ground motions.

Typically, steel jacket structures rely on bracing elements to resist lateral load. Generally, steel braces are used as an economic means of providing lateral stiffness to a steel structure. However, the energy dissipation capacity of a steel-braced structure subjected to earthquake loads is limited due to the buckling of the braces (Tang & Goel, 1988). This is the main reason for most seismic design provisions to recommend smaller response modification factor to a braced frame compared with a moment frame. Recently, the buckling-restrained braces (BRBs) have been widely used to enhance the seismic performance of common building structures (Kiggins & Uang, 2006; Kim & Choi, 2004; Kim & Seo, 2004; Sabellia, Mahin, & Chang, 2003; Sahoo & Chao, 2010; Uang, Nakashima, & Tsai, 2004), tall buildings (Kim, Park, Shin, & Min, 2009) and bridges (Carden, Itani, Buckle, & Aiken, 2004) under seismic loads.

Even though BRBs have not been applied to pile-founded offshore platform structures yet, it is expected that the seismic performance of a FSJOB may be enhanced by using BRBs. The seismic performance of BRBs was verified through many previous analytical (Sabelli, 2000) and experimental (Black, Makris, & Aiken, 2004; Fahnestock, Ricles, & Sause, 2007) studies. Also, current seismic codes and guidelines for building and other structures like American Society for Civil Engineers (ASCE)-7 (2005) give high value for response modification factor for structures with BRB. This implies that a structure with BRB can be designed with smaller seismic base shear than the structure with conventional braces. Also, during the nonlinear range of response, especially in chevron bracing configurations, the small unbalanced vertical brace force between BRBs in tension and compression results in smaller horizontal beam sections (American Institute of Steel Construction, AISC-341, 2005).

*Corresponding author. Email: jkim12@skku.edu

To ensure ductility of platforms in high seismic areas, the American Petroleum Institute Recommended Practice for Planning, Design and Constructing Fixed Offshore Platforms (American Petroleum Institute, API RP-2A, 2000) does not recommend chevron bracing where the ability of a panel to transmit shear is lost if the compression brace buckles. If chevron bracing is to be used, it is recommended that the structural components be designed using twice the strength-level seismic loads. Also, horizontal members should have sufficient capacity to support the redistribution of loads resulting from the buckling of adjacent braces. These requirements for the horizontal beams can be eased if the conventional braces are replaced with BRBs, in which the compressive and tensile strengths are similar to each other and, consequently, the unbalanced force is reduced significantly when they are installed as chevron bracing.

This paper compared the performances of jacket structures with or without BRB designed with three different methods which are the performance-based plastic design, the direct-displacement design method and the force-based design method. As the overall structural response and capacity of pile-founded FSJOP depends primarily on the nonlinear interaction of the foundation with the soil, an analysis model of the jacket considering pile–soil interaction was developed by substituting the soil layers with equivalent elements having pile–soil interaction characteristics. Nonlinear static pushover analysis and nonlinear time-history analysis were carried out to evaluate the performance of the structures. The behaviour factors of the model structures were quantified based on the pushover analysis results, and statistical analysis was conducted to evaluate the central tendencies and dispersion of the important response parameters of the structures.

2. Configuration and analysis modelling of example structures

The platform model considered in this study comprises the deck, the jacket and its appurtenances, and the pile foundation. A perspective plot of the platform is shown in Figure 1(a), a plan view of the jacket is shown in Figure 1 (b), and a 2D-frame model extracted from the platform structure is shown in Figure 1(c). In this study, all analyses are conducted on the representative 2D-frame models. The actual platform has the topside with four stories and a four-story jacket with a total mass of 138,000 tons located in the main nodes of the jacket. The appurtenances include the non-structural members such as flooding system, centraliser, pad-eyes, and plates and stiffeners.

Only the major structural components were included within the analysis model, and the contribution of the conductors to the platforms' stiffness and strength is neglected. The brace elements were modelled as truss elements and Jacket legs were modelled as frame elements (beam–columns). The jacket horizontal members were frame elements (beams) pin-connected at the ends. A pinned beam–column–brace connection was used at all story levels to avoid undesirable connection failures due to unbalanced brace forces. The model structures were designed with compact sections so that local buckling was prevented. The local behaviours of joints were not considered based on the assumption that they were designed to be stronger than elements using larger safety factor.

The mass used in the dynamic analysis consists of the mass of the platform associated with gravity loading defined, the mass of the fluids enclosed in the structure and the appurtenances, and the added mass. The mass of the 2D model frame was calculated by dividing the total mass per floor by the number of frames. The mass of the model frame is applied at each joint, while the mass from the topside structure is applied at the upper two joints of the jacket frame. V-shape braces are used in the short direction. Table 1 shows the characteristics of the platform from which the 2D jacket frame was extracted.

In the present study, the Beam on Nonlinear Winkler Foundation model was used for considering the pile–soil–structure interaction effect (Matlock, 1970). In this model, the parallel nonlinear soil–pile springs were used along the pile penetration length to approximate the interaction between the pile and the surrounding soil. The lateral soil stiffness was modelled using the p–y approach in which, for each layer of soil along the depth, a nonlinear relationship was established between the lateral pile displacement (y) which mobilises the lateral soil reaction (p) per unit length. The procedure of generating p–y curves was recommended in the American Petroleum Institute Standard API RP-2A (2000).

In the present study, p–y curves were based on the actual soil data extracted from the geotechnical report of the platform site (PTTEP International, 2010). In the numerical model proposed in this paper, the multi-linear plastic-type link element in SAP2000 was used to model the nonlinear lateral relation between the soil and the pile. Figure 2(a) shows the configuration of the proposed lateral spring model in SAP2000. A multi-linear kinematic plasticity property type was selected for uniaxial deformation from the SAP2000 library to model the hysteresis of the non-gapping soil behaviour. The skin friction and the end bearing between a pile and the surrounding soil were characterised by a nonlinear force–deformation relationship.

Experimental results suggest that these force–deformation characteristics may be adequately represented by the elastic, perfectly plastic relationship (Anagnostopoulos, 1983; Coyle & Reece, 1966). Frame element was chosen from the library of the SAP2000 to model the behaviour of a pile. The diameter of the pile is uniformly 1210 mm and penetrates into 80 m in the soil. The soil around the pile was simplified into a number of nonlinear

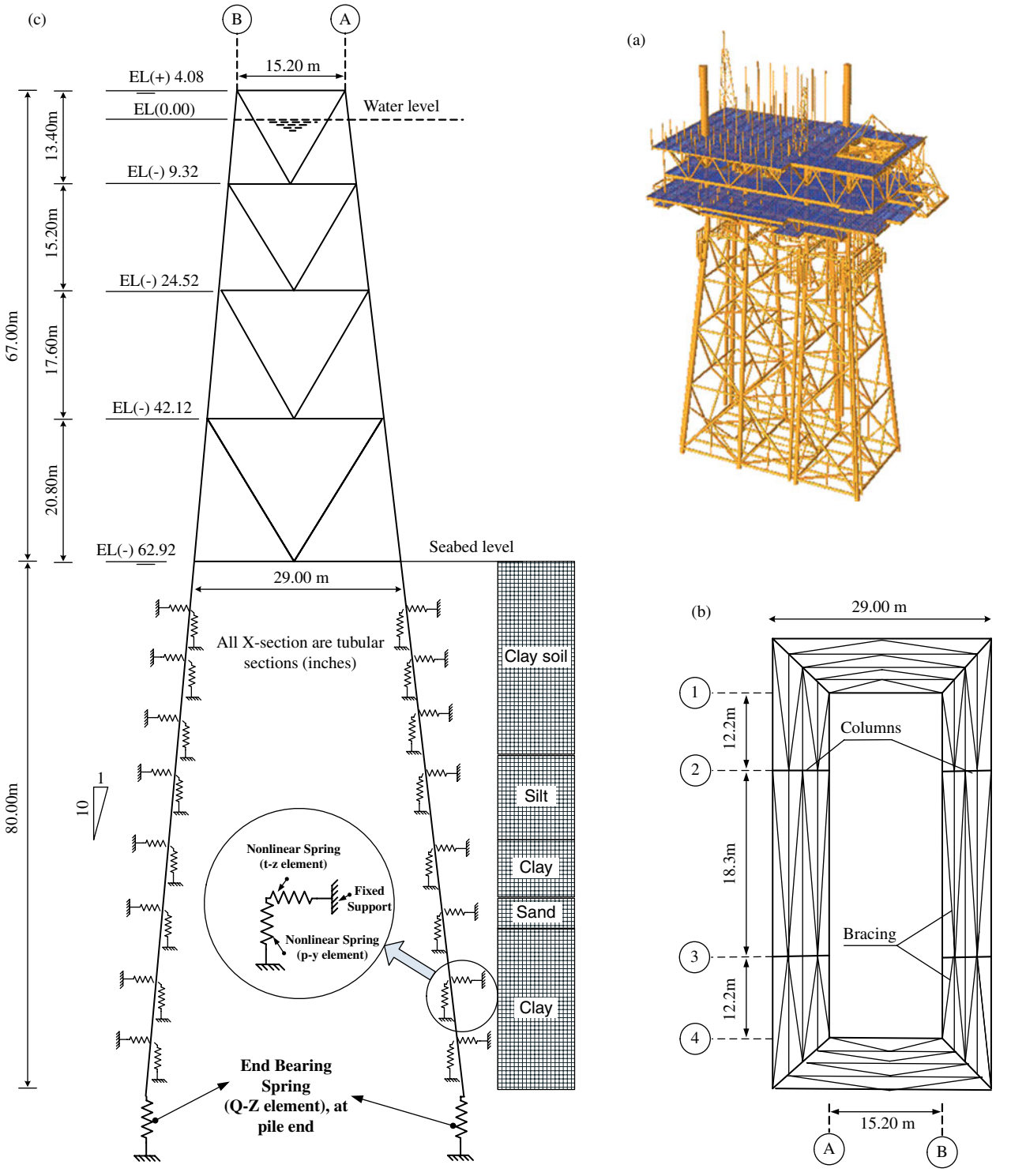

Figure 1. Jacket structure schematic views: (a) perspective plot of the actual platform; (b) plan view of the jacket; (c) 2D single frame extracted from the actual platform with the soil–pile configuration.

vertical springs and an end support spring as shown in Figure 2(b). The spring parameters were calculated according to the site investigation and pile testing data (PTTEP International, 2010).

3. Seismic design of model structures

In order to investigate the best seismic design alternative of BRB in FSJOB, the jacket structures with V-shaped BRBs were designed based on three different methods

Table 1. Characteristics of the platform.

Item	Description
Water depth	62.92 m
Jacket height	67.00 m
Jacket plan dimensions	15.2 m × 42.7 m
Number of jacket legs	8
Total mass	13,800 ton m

such as the performance-based plastic design (PD) (Goel & Chao, 2008; Sahoo & Chao, 2010), the direct displacement-based design (DBD) method (Priestley, 2000; Priestley, Calvi, & Kowalsky, 2007) and the force-based (or code-based) (FB) design (AISC-341, 2005; AISC-360, 2005). For comparison, another model structure with a conventional bracing was designed following the force-based procedure (FB-Conv).

Figure 3 depicts the response spectra of the earthquakes obtained from the geotechnical earthquake engineering report for the site, Gulf of Moattama (PTTEP International, 2010). The maximum considered earthquake (MCE) response spectrum was used for seismic design of the model structures. For each model case, the satisfaction of the API-RP2A seismic criteria for strength and ductility was checked. Table 2 summarises various parameters used to compute the design base shear for the different methods.

3.1 *Force-based design*

The design base shears of the model structures FB-Conv and FB–BRB with conventional and BRB bracing, respectively, were obtained in accordance with ASCE-7 (2005). The two structures were considered as an ordinary concentric braced frame with R factor of 3.25 and a buckling-restrained braced frame with non-moment-resisting beam–column connections with R factor of 7, respectively. The seismic design base shear was computed using the site-specific response spectrum which corresponds to 2/3 of the MCE with 2% probability of occurrence in 50 years in the Gulf of Moattama, offshore of Myanmar, shown in Figure 3.

Table 2(a) presents the values of the base shear coefficients and other important parameters. The design base shear coefficients for the conventional and the BRB frames are 0.11 and 0.052, respectively. The difference in the base shear coefficients is mainly caused by the

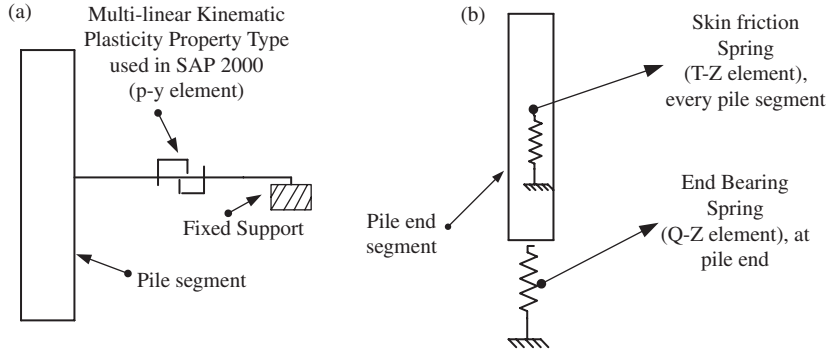

Figure 2. Schematic illustration of soil–pile interaction modelling in SAP2000: (a) configuration of lateral soil stiffness; (b) vertical and end-bearing spring models.

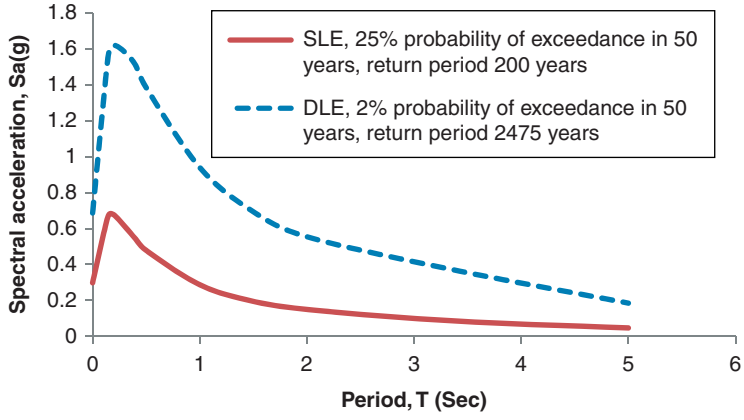

Figure 3. Response spectra used for the strength- and ductility-level seismic design.

Table 2. Design parameters for model structures.

(a) FB–BRB and FB-Conv models	
S_{DS} (g)	1.0
S_{D1} (g)	0.7
Framing type	BRBF (FB–BRB) OCBF (FB-Conv)
Response modification factor, *R*	7 (FB–BRB) 3.25 (FB-Conv)
Importance factor, I	1
Occupancy category	II
Seismic design category	D
Base shear coefficient, *V*/*W*	0.052 (FB–BRB) Base shear = 1941 kN 0.11 (FB-Conv) Base shear = 4107 kN
Fundamental period (s)	2.79 (FB–BRB) 3.1 (FB-Conv)
(b) PD–BRB model	
Parameters	Description/value
Target drift ratio, Δ_u (%)	1.75
Total frame height, *H* (m)	67.00
Yield drift ratio, Δ_y (%)	0.63 ((0.2 + *H*/155))
Fundamental period (s)	1.92
Inelastic drift ratio, Δ_p (%)	1.12 (Δ_u (%) − Δ_y (%))
Ductility reduction factor, R_μ	2.7
Structural ductility factor, μ_s	2.7 (Δ_u (%)/Δ_y (%))
Response modification factor, *R*	7
Energy modification factor, γ	0.6 ($(2\mu_s - 1)/R_\mu^2$)
Spectral acceleration, S_a (g)	0.367
Seismic weight, *W* (kN)	37,340
Base shear coefficient, *V*/*W*	0.06
Base shear, *V* = 2235 kN	
Material over-strength factor, R_y	1.1
Compression strength adjustment factor, β	1.15
Strain hardening adjustment factor, ω	1.25
Fundamental period (s)	2.98
(c) DBD–BRB model	
Target drift, Δ_u (m)	1.2 (1.75%*H*)
Damping	$\zeta_{eq.} = \zeta_{eq} + \zeta_{hyst.} = 0.05 + 0.15 = 0.2$
Yield drift ratio, Δ_y (%)	0.63
Ductility factor, μ_s	2.7
T_{eff} (s)	4.0
M_{eff} (kN s^2/m)	3271
Effective stiffness (kN/m)	7000
Initial stiffness (kN/m)	18,856
Base shear coefficient, *V*/*W*	0.09 (base shear = 3360 kN)
Fundamental period (s)	2.4

difference in the *R* factors. The distribution of the base shear along the height is based on the formula proposed in the ASCE7-05.

For force-based design of the structures in accordance with the ASCE-7, the nominal yield strength, f_y, of materials used for all elements is set to be 55 ksi with the value of material overstrength factor, R_y, of 1.1. The steel core areas of BRBs are calculated using the following relation suggested in the AISC341-05:

$$P_u < P_{ysc}, \quad (1)$$

where P_u is the required axial strength and ϕ is the strength reduction factor, which is 0.9 for both tension and compression, P_{ysc} is the design strength which is equal to F_yA_{sc} in which F_y and A_{sc} are the specified minimum yield strength and net area of steel core, respectively.

In the FB–BRB model, the demand on beams and columns is obtained based on the expected yield and ultimate strengths of BRBs in tension and compression by applying material overstrength factor, R_y, compression adjustment factor, β, and the strain-hardening adjustment factor, ω. The values of these factors are shown in Table 2(a). In the case of conventional braces, the demands on beams and columns were obtained based on the expected tensile yield and buckling strength of braces in tension and compression, respectively, by applying material overstrength factor, R_y.

3.2 *Performance-based plastic design*

The design concept here uses pre-selected target drift and yield mechanism as design criteria. In this method, the design base shear is computed using an energy–work balance concept where the energy needed to push an equivalent elastic–plastic single-degree-of-freedom system up to the target drift level is calculated as a fraction of elastic input energy obtained from the selected elastic design spectra. Reduction in strength and stiffness at the higher inelastic deformation levels, which reflects the reduction in energy dissipation capacity, can also be accounted for in the design by using an energy reduction factor η. As BRBs exhibit full and stable hysteretic response, the value of η can be assumed as unity.

In this method, the inelastic characteristics of structural components are directly considered in the design to achieve the desired performance objectives (Goel & Chao, 2008). This design method has been applied to other steel structural framing systems in previous studies (Chao & Goel, 2005, 2008). The detailed methodology for extracting the design base shear can be found elsewhere (Goel & Chao, 2008; Sahoo & Chao, 2010). A yield drift ratio, Δ_y, is assumed to be equal to (0.2 + *H*/155) = 0.63%, where the total frame height (*H*) is 67.0 m, and a target drift level of 1.75% is selected which leads to structural ductility factor, $\mu_s = \Delta_u/\Delta_y$, equal to 2.7. The value of ductility reduction factor, R_μ, for a structural system can be determined by using the R_μ–μ_s–T relationship proposed by Newmark and Hall (1982). The energy modification factor γ is equal to $(2\mu_s - 1)/R_\mu^2$, which is 0.6.

The spectral acceleration, S_a = 0.367 g, can be obtained based on the ASCE7-05 by multiplying the corresponding MCE response spectrum value (at the assumed natural period

of the structure) by 2/3. In the present study, MCE corresponds to the ductility-level earthquake (DLE, 2% probability of exceedance in 50 years). Based on Table 2(b), the base shear coefficient, *V/W*, was computed to be 0.06, and the base shear was 2235 kN. These values are slightly higher than those of the FB–DBD model. The shear distribution factor at the *i*th level, β_i, was calculated as follows:

$$\beta_i = \sum_{j=i}^{n} \left(\frac{w_j.h_j}{w_n.h_n} \right)^{0.75T^{-0.2}}, \quad (2)$$

where w_j is the seismic weight at the *j*th level, h_i is the height at the *i*th level from the base, h_j is the height at the *j*th level from the base, h_n is the height of roof level from the base and w_n is the seismic weight at roof level. The detailed calculation of the shear distribution factor, β_i, can be found elsewhere (Chao, Goel, & Lee, 2007). The shear distribution factors along the structure levels are, starting from the first story, 0.025, 0.075, 0.09 and 0.81, respectively.

3.3 Displacement-based design

The fundamental philosophy behind DBD is that structures are designed to achieve a specified performance level, defined by strain or drift limits, under a specified level of seismic intensity. The fundamentals of DBD have been presented in many previous publications (Priestley, 2000; Priestley et al. 2007). DBD method characterises the structure by the secant stiffness K_e at a target drift, Δ_u, and a level of equivalent viscous damping ratio, $\zeta_{eq.} = \zeta_{eq} + \zeta_{hyst}$, representative of the combined elastic damping and the hysteretic damping energy absorbed during inelastic response (Priestley, 2000).

The procedure includes selection of a target drift and determination of the required effective stiffness of a substitute elastic single degree of freedom system using the system ductility and the equivalent damping. Subsequently, the required effective strength is determined based on the effective stiffness and the target displacement. The required initial stiffness and elastic strength are calculated based on the effective stiffness and strength considering the ductility and overstrength characteristics. Finally, members are designed to achieve the required stiffness, strength and ductility (SEAOC, 1999).The DBD procedure applied to the model structure is as follows:

Step 1: The target drift ratio is assumed as $\Delta_u = 1.75$ (%), which is 1.2 m.
Step 2: The effective period is determined with an equivalent damping value (including hysteretic damping, assumed 15% of critical, and the traditional 5% viscous damping), then, by entering the displacement response spectrum chart knowing Δ_u, the effective period T_{eff} is obtained.
Step 3: The effective stiffness is determined as $Ke = 4\pi^2 M_e / T_{eff}^2$, where M_e, the effective mass, can be obtained using the following equation knowing the mass at each story, m_i, and the amplitude of the first mode shape at the same story, Δ_i:

$$M_e = \frac{\left(\sum_{i=1}^{n} m_i.\Delta_i\right)^2}{\left(\sum_{i=1}^{n} m_i.\Delta_i^2\right)}. \quad (3)$$

Step 4: The required initial stiffness is determined as $K_i = \mu_s K_e$ where μ_s is the ductility factor given in Table 2(c).
Step 5: The required strength (the design base shear) is obtained as $V_{base} = K_e \Delta_u$. The base shear coefficient is shown in Table 2(c).
Step 6: The required yield strength is obtained by $V_y = V_{base}/\Omega$, where Ω is the system overstrength factor which is 2.5.

In the DBD–BRB model, the cross-sectional area of the BRB was determined to achieve the required inter-story drift ratio (IDR) limits (1.75% of the story height). This led to higher design base shear than those of the other models with BRB, and justified the large BRB cross-sectional area compared with other models. Table 3

Table 3. Details of the tubular sections and BRBs used in the model structures.

Members	Story	PD–BRB	DBD–BRB	FB–BRB	FB-Conv
			Area (cm^2) or diam.(cm) × thick (cm)		
Braces	1	60.8	106.8	50.9	55 × 2.5
	2	60.8	106.8	50.9	60 × 2.2
	3	60	106.8	46.3	50 × 2.6
	4	53.4	106.8	40.7	50 × 2.2
Columns	1	90 × 5.25	100 × 5.25	95 × 5.0	110 × 5.0
	2	90 × 4.0	100 × 4.0	95 × 4.0	100 × 4.5
	3	80 × 4.0	85 × 3.8	80 × 3.8	90 × 4.0
	4	75 × 3.4	75 × 3.4	75 × 3.2	90 × 4.0
Beams	1	80 × 4.0	80 × 4.5	75 × 4.6	75 × 4.5
	2	75 × 4.0	75 × 4.4	75 × 3.6	80 × 4.2
	3	75 × 3.5	75 × 3.5	70 × 3.4	75 × 4.0
	4	65 × 3.0	65 × 3.0	55 × 2.75	50 × 2.5

Table 4. Dynamic characteristics of the structural models.

	PD–BRB			DBD–BRB			FB–BRB			FB-Conv.		
Mode	1	2	3	1	2	3	1	2	3	1	2	3
Natural periods (s)	2.8	0.9	0.5	2.42	0.74	0.44	2.75	0.86	0.47	1.8	0.45	0.4
Mass participation factor	0.83	0.07	0.01	0.83	0.06	0	0.83	0.06	0.01	0.8	0.9	0

summarises the details of the tubular sections and BRBs used in the model structures. The dynamic characteristics of each model are shown in Table 4.

3.4 Comparison of base shear computation methods

In the force-based designed method, no inelastic behaviour was introduced in the base shear calculation. In the PD method, the base shear was calculated based on parameters reflecting the inelastic behaviour of the model, such as the energy modification factor which includes the ductility reduction factor and the structural ductility factor. Also, the reduction in the energy dissipating capacity was accounted for in the design by using the energy reduction factor. This factor was assumed as unity in the current study, as the BRBs exhibit full and stable hysteretic response.

Among the other parameters used were the target drift and the modal properties. In the DBD method, the base shear was calculated considering the hysteretic damping, system overstrength, required initial stiffness and the system ductility factor. Considering those parameters during the design phase resulted in more realistic results. The elastic fundamental period was used in all base shear calculation except for the DBD model. In the latter model, the effective period of the structures was used in the design which is considered as the real elongated period of the model at the target drift.

3.5 Verification of API seismic design requirements

After designing the models using the lateral load determined from each design method, the API RP-2A (2000) seismic design requirements for fixed offshore platforms were checked, which are the strength requirement for a strength-level earthquake (SLE, 25% probability of exceedance in 50 years, return period 200 years) and the ductility requirement for a DLE (2% probability of exceedance in 50 years, return period 2475 years). Ductility seismic design was intended to ensure that the platform has sufficient reserve capacity to prevent its collapse during rare, intense earthquake motions. Representative set of ground motion records that have characteristics of rare, intense earthquakes at the site were developed from a site-specific seismic hazard study following the provisions of API RP-2A (2000).

The complete quadratic combination (CQC) method was used for combining modal responses. Four vibration modes having the highest overall response were considered for an adequate representation of the 2-D jacket frame response. The P-delta effect of gravity loads acting through lateral deflection of the structure was considered in the analysis. It should be demonstrated that the platform remains stable under the loads imposed by these ground motions. The platform was considered unstable when the deflections were large enough to cause collapse under the influence of gravity loads. In the present study, nonlinear dynamic time-history analyses were conducted using four representative earthquake ground motion records to check the stability of the model structures. These records are based on the DLE response spectrum of the platform site. The response spectra of the selected records are shown in Figure 4, and the characteristics of the records are summarised in Table 5.

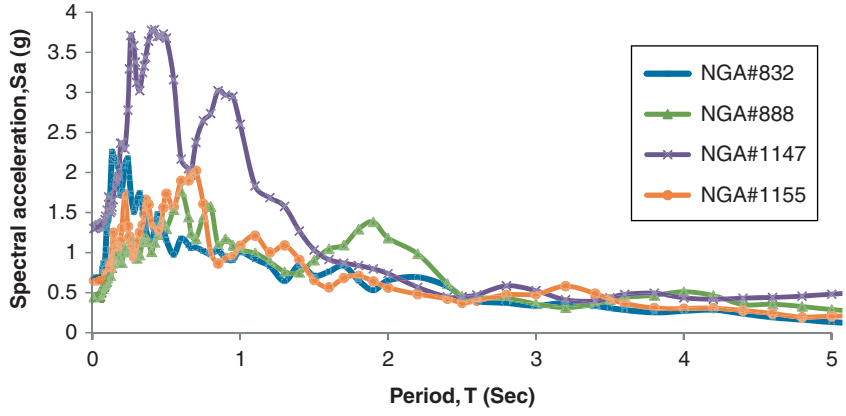

Figure 4. Response spectra of the DLEs used to check stability of the model structure.

Table 5. Characteristics of the ground motion suite used in the NLTH analysis.

	No	NGA number[a]	Scale factor	Event	Station	Mag.	R_{jb}[b] (km)	R_{rup}[c] (km)
DLE	1	832[d]	4.5	Landers	Amboy	7.28	69.2	69.2
	2	860	30.2	Landers	Hemet Fire Station	7.28	68.7	68.7
	3	886	71.7	Landers	Puerta La Cruz	7.28	94.5	94.5
	4	888[d]	5.6	Landers	San Bernardino – E & Hospitality	7.28	79.8	79.8
	5	891	35.5	Landers	Silent Valley – Poppet Flat	7.28	50.9	50.9
	6	114[d]	5.4	Kocaeli – Turkey	Ambarli	7.51	68.1	69.6
	7	1149	12.8	Kocaeli – Turkey	Atakoy	7.51	56.5	58.3
	8	1154	16.9	Kocaeli – Turkey	Bursa Sivil	7.51	65.5	65.5
	9	115[d]	6.3	Kocaeli – Turkey	Bursa Tofas	7.51	60.4	60.4
	10	1163	7.7	Kocaeli – Turkey	Hava Alani	7.51	58.3	60.0
SLE	11	1627	10.6	Caldiran – Turkey	Maku	7.21	50.8	50.8
	12	1637	2.4	Manjil – Iran	Rudsar	7.37	64	64.5
	13	1640	1.8	Manjil – Iran	Tonekabun	7.37	93.3	93.6
	14	1766	5.7	Hector Mine	Baker Fire Station	7.13	64.1	64.8
	15	1767	8.5	Hector Mine	Banning – Twin Pines Road	7.13	83.4	83.4
	16	1773	3.2	Hector Mine	Cabazon	7.13	76.9	76.9
	17	1776	5.4	Hector Mine	Desert Hot Springs	7.13	56.4	56.4
	18	1782	7.5	Hector Mine	Forest Falls Post Office	7.13	74.9	74.9
	19	1783	6.4	Hector Mine	Fort Irwin	7.13	65	65.9
	20	1786	5.4	Hector Mine	Heart Bar State Park	7.13	61.2	61.2

[a] Next generation of ground-motion attenuation models.
[b] Joyner–Boore distance (km): the horizontal distance to the surface projection of the rupture plane.
[c] Closest distance (km) to the fault rupture plane.
[d] Used for DLE design.

The modal damping ratio of 5% of critical damping was used in the analyses.

For the design load cases, the API-RP2A requires that earthquake load should be imposed on the platform as a separate environmental loading condition, i.e. no wave, current or wind loads are combined with the seismic loads. In the present study, seismic loading was found to be the governing design loading condition for the platform. After designing each model and checking the API-RP2A requirements, the member cross sections were refined. Table 6 shows the total volume of structural steel used for each model. The PD–BRB model was designed with the smallest amount of steel, whereas the FB-Conv model was designed with significantly larger amount of steel compared with other model structures. For each model, the K-bracing connection was designed to satisfy the requirements of allowable joint capacity according to item 4.3.2 in API-RP2A (API RP-2A, 2000).

Fixed steel jacket platforms are commonly constructed or fabricated on onshore yards with the same construction conditions of conventional modular steel structures. There are some new BRB configurations that may be suitable for tubular elements of fixed steel jacket platforms such as proposed by Yin, Wang, and Li (2009), who proposed a double-tube BRB with contact ring. The maintenance or strengthening of BRB in fixed steel jacket platforms can be treated as conventional damaged tubular elements under seawater. The BRB can be fitted with a grouted clamp over the damaged areas. Once the grout plug is set, an ordinary Portland cement and seawater mix is injected into the annulus for structural integrity. Such a clamp is designed with bolt-together sections and is equipped with primary and secondary grout inlets.

Table 6. Total volume of structural steel used for each model.

Model	Steel volume (m^3)
FB–BRB	20.8
PD–BRB	19.6
DBD–BRB	22.2
FB-Conv.	28.9

4. Seismic performance evaluation of model structures

4.1 Nonlinear static analysis results

In this section, the nonlinear static analyses of the model structures were carried out by applying lateral load pattern based on the first vibration mode. Figure 5 shows the nonlinear load–deformation relationship of the BRB and conventional brace elements recommended in the Federal Emergency Management Agency (FEMA)-356 (2000) with the acceptance criteria such as Immediate Occupancy (IO), Life Safety (LS), Collapse Prevention (CP) and Collapse (C) shown on the curves. In the load–deformation relationships, P_y and P_{cr} represent the yield force and the buckling strength, respectively, and $\Delta_y = (P_y L)/(EA)$ and $\Delta_{cr} = (P_{cr} L)/(EA)$ denote the axial deformation corresponding to the first yield and the buckling strength, respectively; $P_y = F_y A$; P_{cr} is the

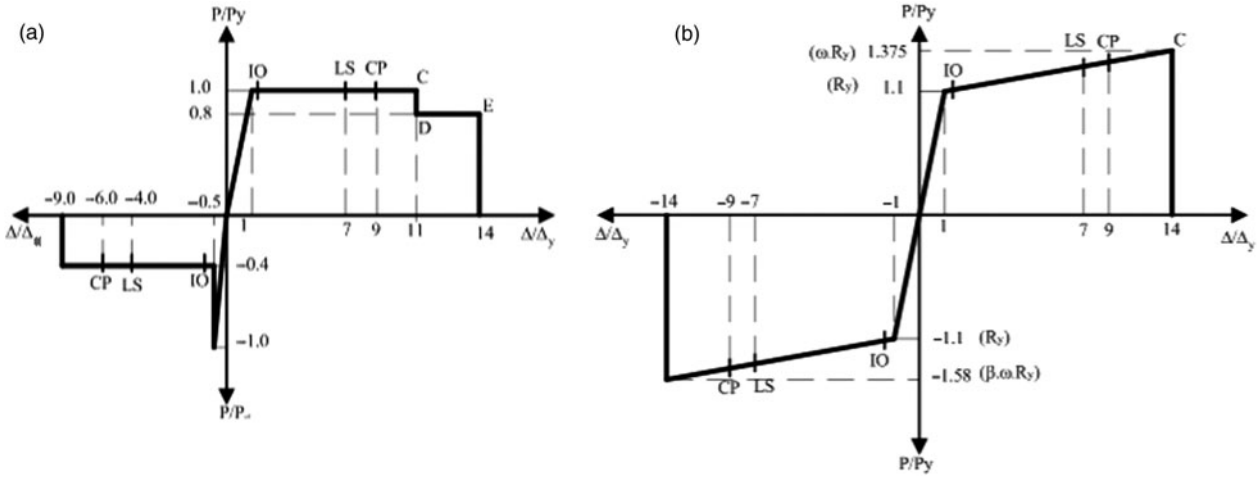

Figure 5. Force–deformation relationship of a plastic hinge defined in SAP2000: (a) conventional brace; (b) BRB.

buckling load calculated according to the AISC Chapter E; L is the member length; E is the material modulus of elasticity; and A is the cross-sectional area of the element. The adjusted brace strength factors for BRBs (R_y, β and ω), were determined according to AISC-341 as shown in Table 2.

Figure 6(a) depicts the pushover curves of the model structures with indication of the design base shears and Figure 6(b) shows the maximum strength of each model structure. It can be observed that the overall nonlinear behaviours of the models with BRB designed with three

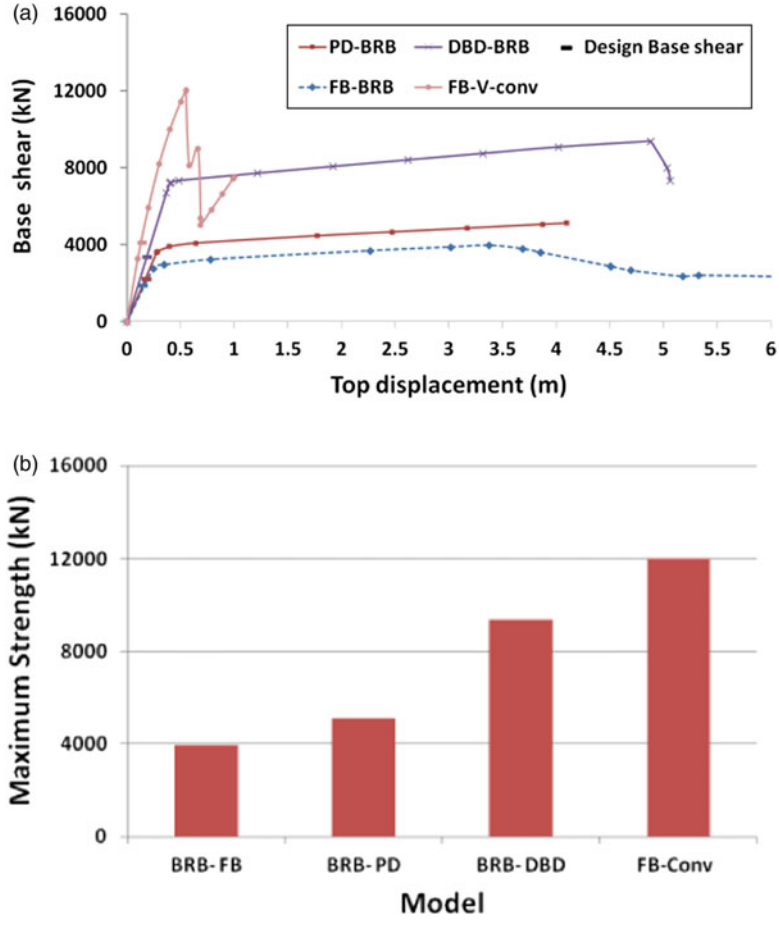

Figure 6. Pushover analysis results of the model structures: (a) pushover curves; (b) maximum strength.

different methods are similar except the difference in strength. The figure also shows that, compared with the structure with conventional bracing, the structures with BRB turned out to have significantly increased deformation capacity. Furthermore, it is noticed that the yield strength of structures designed using BRB is much smaller than that of the structures designed using conventional braces. The stiffness and strength of the DBD–BRB model are much larger than those of the PD–BRB and the FB–BRB models due to the increase in the cross-sectional area of BRB to meet the target displacement.

The initial stiffness and the strength of the FB–BRB are slightly smaller than those of the PD–BRB owing to the smaller brace sections. After yielding, the models with BRB behave stably until the lateral load-resisting capacity of the structure start to decrease rapidly at the maximum inter-story drift ratios (MIDR) of 6.0%, 7.2% and 5.0% for PD–BRB, DBD–BRB and FB–BRB models, respectively. The failure points are much larger than the target drift, 1.75% of the story height, assumed in the design stage. In the FB-Conv, however, the strength dropped significantly before the limit state is reached as a result of buckling of braces.

Figure 7 shows the plastic hinge distribution in the model structures at the target drift indicating the IO, LS, CP and C damage states. A uniform distribution pattern of plastic hinges in all the BRB was observed in the DBD–BRB model at the target drift. In this model, all plastic hinges reached the IO limit state. For PD–BRB and FB–BRB models, the IO limit state was reached with less number of plastic hinges compared with the DBD–BRB model. However, the plastic hinges spread to wider region compared with the FB-Conv case. This introduces higher energy dissipation capability in the BRB models compared with the conventional braced one. In the case of FB-Conv, local failure mechanism formed at the second story level with formation of plastic hinges in the beams. This is attributed to the large unbalanced force resulted from the buckling of braces.

The distribution of plastic hinges at the maximum strength is plotted in Figure 8. In all models with BRB, the inelastic deformation spread to all stories, which resulted in significant ductility. On the other hand, the overall ductility of the FB-Conv model is quite limited as the inelastic deformation is concentrated at the third story. It can be observed that the C limit state was reached in all models with BRB. The distribution of plastic hinges at the point right after reaching the maximum strength is plotted in Figure 9. At this stage, plastic hinges corresponding to the IO limit state formed in the third story horizontal beam in the DBD–BRB model, whereas, in the PD–BRB and the FB–BRB models, the deformations of all BRBs in the fourth story exceed the collapse level to form a

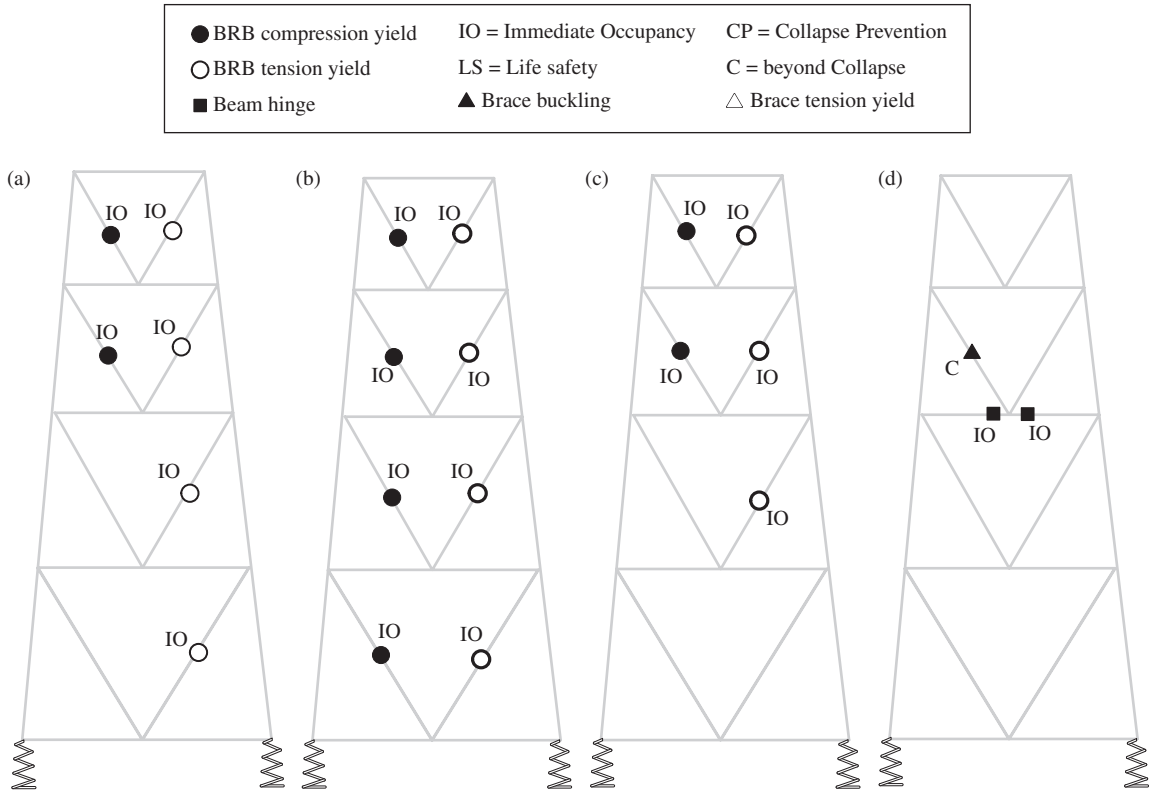

Figure 7. Plastic hinge formation at the target displacement of 1.75% of the jacket height: (a) PD–BRB; (b) DBD–BRB; (c) FB–BRB; (d) FB-Conv.

mechanism. The analysis results show that by preventing localised damage in the frame, the ductility of the structures can be improved significantly.

4.2 *Effect of lateral load pattern on the pushover analysis results*

Structures designed according to current code procedures with large R values are expected to undergo large deformations in the inelastic range when subjected to major earthquakes. The commonly used lateral force patterns in current practice depend on the elastic mode shape and fundamental period of the structure, and do not explicitly consider the large deformation. The load pattern is close to a straight line when $T < 0.5$ s and is close to a parabola when $T \geq 2.5$ s. In the performance-based PD method, a more realistic design lateral force distribution is used, which represents the peak lateral force distribution in the structure in the inelastic state and includes the higher mode effects.

In the DBD method, the load pattern is determined so that the selected yield mechanism is developed at the target inter-story drift. It was observed in the previous section that plastic hinges formed concentrated at the upper half of the jacket structure in the cases of the PD–BRB, FB–BRB and the FB-Conv at the target displacement. In the FB-Conv model, all plastic hinges formed only at the upper two stories. In the PD–BRB and the FB–BRB models, many plastic hinges deformed beyond the IO limit to the CP and C limits in the upper two stories, whereas in the lower two stories they hardly reached the IO limit. Table 7 shows the design lateral load pattern as a percentage of the design base shear for each model. It is noticed from the table that the DBD method gives a more uniform load pattern which led to uniform capacities of the BRB and, consequently,

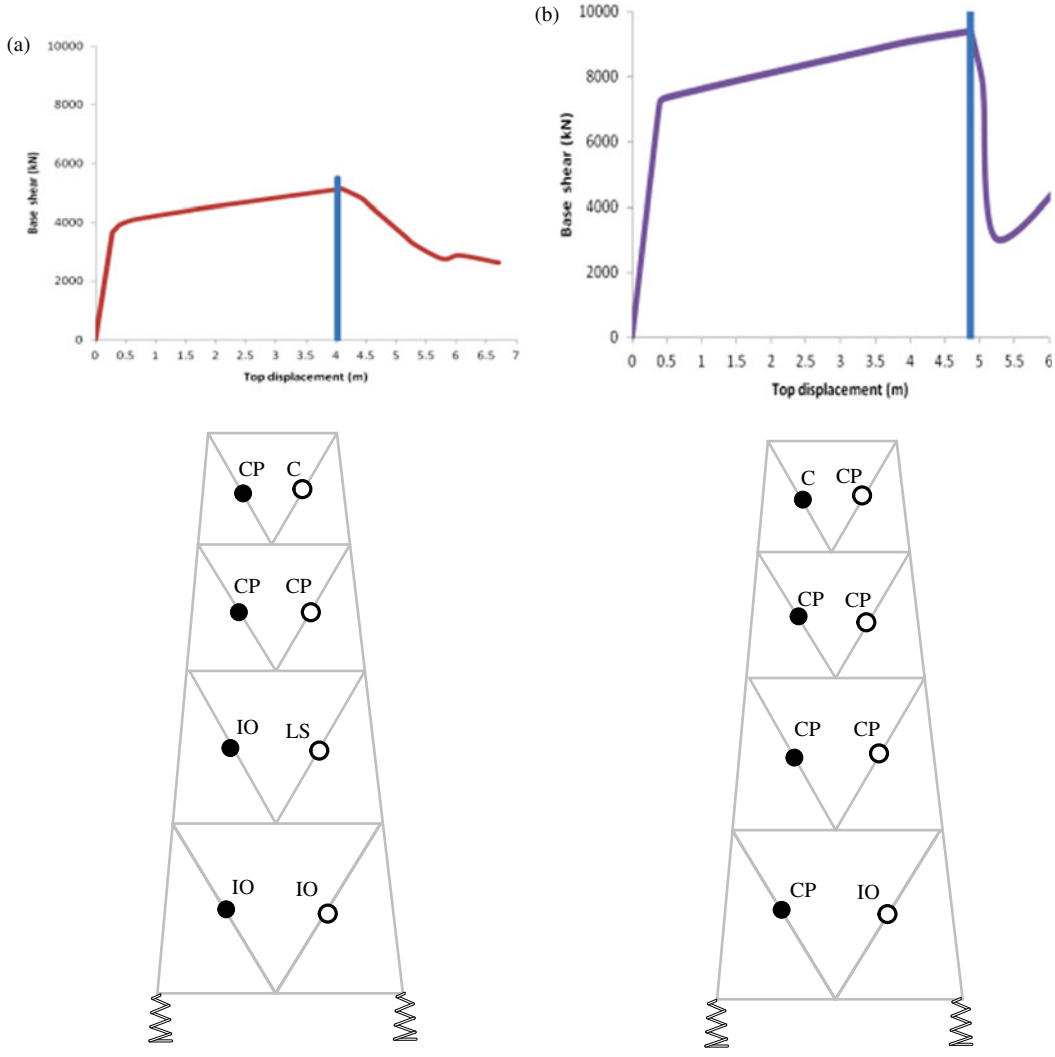

Figure 8. Plastic hinge formation in the models at the maximum strength: (a) PD–BRB (at 4.03 m), @MIDR = 6%; (b) DBD–BRB (at 4.87 m), @MIDR = 7.2%; (c) FB–BRB (at 3.37 m), @MIDR = 5%; (d) FB-Conv (at 0.6 m)@MIDR = 1.9%.

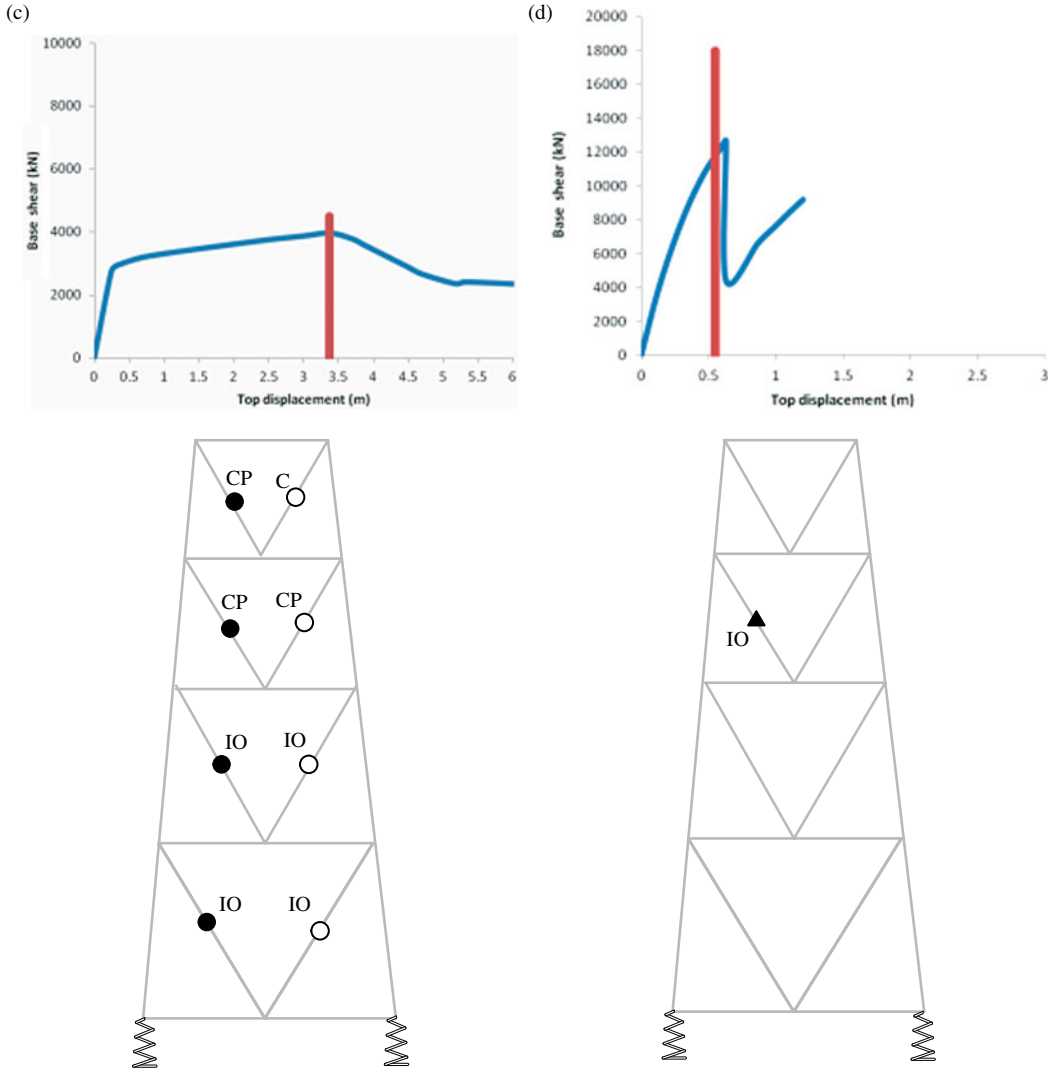

Figure 8. *(Continued).*

a more uniform plastic hinge distribution at the intended drift level.

4.3 Behaviour factors of the model structures

Based on a typical structure idealised pushover curve, Applied Technology Council (ATC)-19 defines the overstrength factor R_o and the ductility factor R_μ as follows (Osteraas, 1990):

$$R_o = \frac{V_y}{V_d}, \quad R_\mu = \frac{V_e}{V_y}, \tag{4}$$

where V_d is the design base shear, V_e is the maximum seismic demand for elastic response and V_y is the base shear at yield. An overstrength factor represents three different components which are, according to FEMA-450 (2004), design overstrength, material overstrength and system overstrength. The ductility factor is the ratio of the maximum displacement that is reached by the stable model structure divided by the model yield displacement. The response modification factor is computed by multiplying the overstrength and the ductility factor as recommended by the ATC-19 (1995).

Figure 10 shows the overstrength, ductility and the response modification factors of each model structure obtained from the pushover analysis results. The overstrength factor, which is the ratio of the yield to design strength, is 3.0 for the FB-Conv model. However, the overstrength factors of the structures with BRB are 1.18 (PD–BRB), 2.14 (DBD–BRB) and 1.07 (FB–BRB), which are significantly smaller than those of the structure with conventional braces. The smaller overstrength factors of the structures designed using BRB are primarily contributed from the fact that the structures are more optimally designed in such a way that structural damages are more uniformly distributed throughout the stories.

It is also observed that the overstrength factor of the DBD–BRB model is almost twice those of the other BRB models. This is because at the design stage of DBD–BRB model, the cross-sectional areas of BRB were further increased to maintain the target drift ratio, IDR = 1.75%. The ductility factors of the PD–BRB and the DBD–BRB are slightly larger than that of the FB–BRB. This is due to the higher concentration of plastic hinges at the upper stories in the FB–BRB model as shown in Figure 7, which led to a formation of a failure mechanism in the fourth story with all plastic hinges reaching the failure limit state C as shown in Figure 9. In the FB-Conv model, a brittle behaviour was observed as a result of the concentration of plastic hinges in a story. This led to a local failure mechanism formed in this level, which resulted in a smaller ductility factor. The response modification factors of the model structures with BRB range from 9.0 to 21.5, which are significantly larger than the design response modification factor of 7.0 used in this study. Generally, the models with BRBs retain a superior seismic load-resisting capacity, and the DBD–BRB model, in particular, showed the largest R-factor. The FB-Conv model showed lower value of R-factor than that used in the design stage.

4.4 *Effect of the soil–pile interaction*

Table 8 presents the maximum inter-story drift of the model structures at the target displacement (1.2 m), where the effect of the soil–pile interaction on the maximum inter-story drift is observed in all cases except for the FB–BRB. No difference was observed in responses between the fixed and hinged support conditions in all models. It is noticed from the pushover curves shown in Figure 11 that the structures with fixed and hinged end conditions have almost identical pushover curves. On the other hand, there is a significant change in the behaviour of the structure

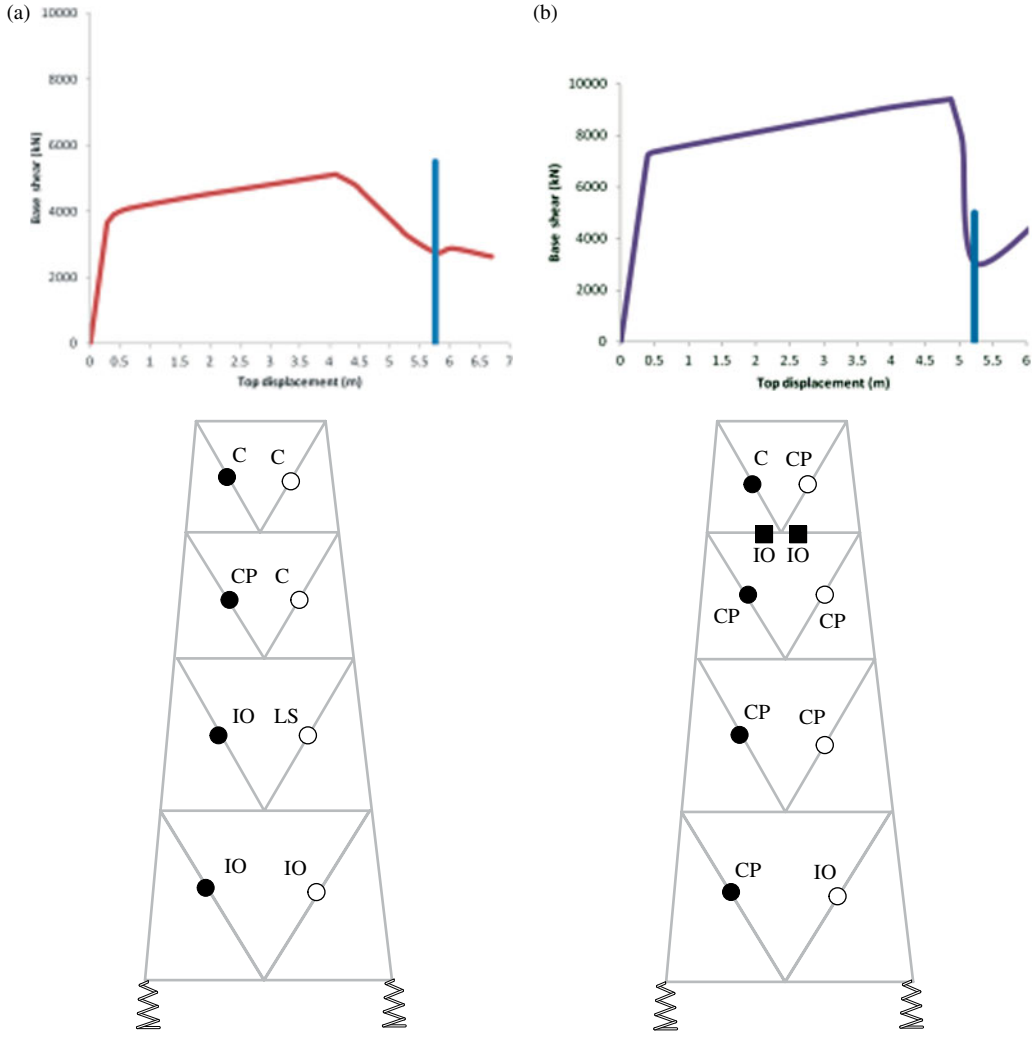

Figure 9. Plastic hinge formation at the negative stiffness: (a) PD–BRB (at 5.76 m), @MIDR = 8.5%; (b) DBD–BRB (at 5.23 m), @MIDR = 7.8%; (c) FB–BRB (at 4.5 m), @MIDR = 6.7%; (d) FB-Conv (at 0.63 m), @MIDR = 2.0%.

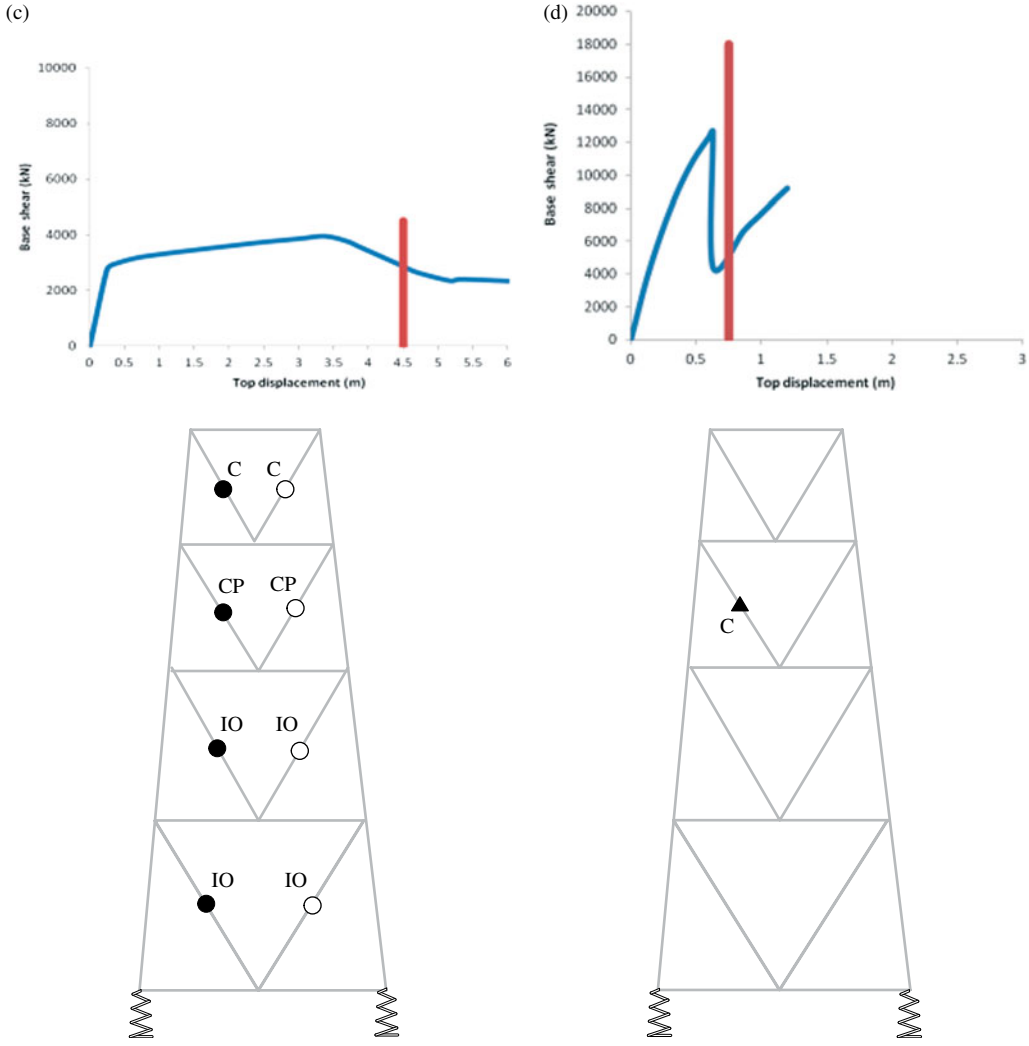

Figure 9. *(Continued).*

with conventional braces. It is noticed that the more strength is introduced in the jacket lateral resisting system (as in the case of the FB-Conv), the sensitivity of the structural responses depends more heavily on the soil–pile system. Obviously, the more ductility the jacket has, the less soil–pile interaction affects the global response. This can be better understood by further investigating the relative stiffness ratio between the soil–pile system (sub-structure) and the jacket lateral load-resisting system (super-structure), which is referred to as the relative

Table 7. Design lateral force pattern as a percentage of design base shear.

Story	PD–BRB	DBD–BRB	FB–BRB	FB-Conv
4	0.81	0.62	0.81	0.79
3	0.09	0.13	0.11	0.12
2	0.08	0.13	0.06	0.07
1	0.02	0.12	0.02	0.02

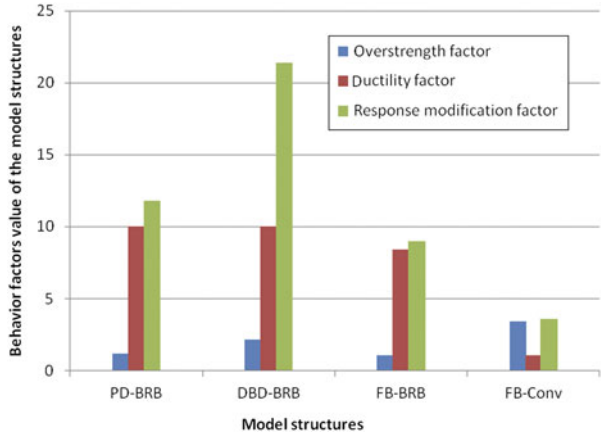

Figure 10. Behaviour factors of the model structures obtained from pushover analysis.

Table 8. Maximum inter-story drift at the target displacement (%).

Model	Soil–pile interaction	Fixed ends	Hinged ends
PD–BRB	3.1	3.7	3.7
DBD–BRB	2.0	2.6	2.4
FB–BRB	3.7	3.7	3.7
FB-Conv	5.46	5.9	5.9

stiffness index (I) as follows:

$$I = \frac{K_{\text{sub-structure}}}{K_{\text{super-structure}}}, \tag{5}$$

where $K_{\text{sub-structure}} = V_{\text{base}}/\Delta_{\text{pile tip}}$ and $K_{\text{super-structure}} = V_{\text{base}}/\Delta_{\text{jacket top}}$.

Figure 12 presents a simplified schematic model for the jacket and the pile–soil system. The relation between the base shear and the relative stiffness index (I) for all models is depicted in Figure 13, where the slope of the curve indicates how much the sub-structure contributes to the global response of the structure. The conventional brace model showed the steepest slope, whereas the models with BRB showed smaller slopes. This implies that the sub-structure has more effect on the global response in the case of FB-Conv than on the BRB models. In the case of BRB models, after the maximum strength is reached, the steepest slope is noticed in the DBD–BRB, whereas the lowest is observed in the FB–BRB. Therefore, to quantify the contribution of the soil–pile system to the global seismic response, it is important to evaluate the relative stiffness ratio between the super- and the sub-structures. Based on the stiffness index, it can be decided whether to consider the soil–pile system in detail or to use a well-defined fixed or hinged end condition. In the case of the systems with large ductility like models with BRB, the effect of soil–pile nonlinear interaction is marginal on the response of the super-structure. However, the soil–pile interaction effect is significant in the structure with conventional bracing having limited ductility.

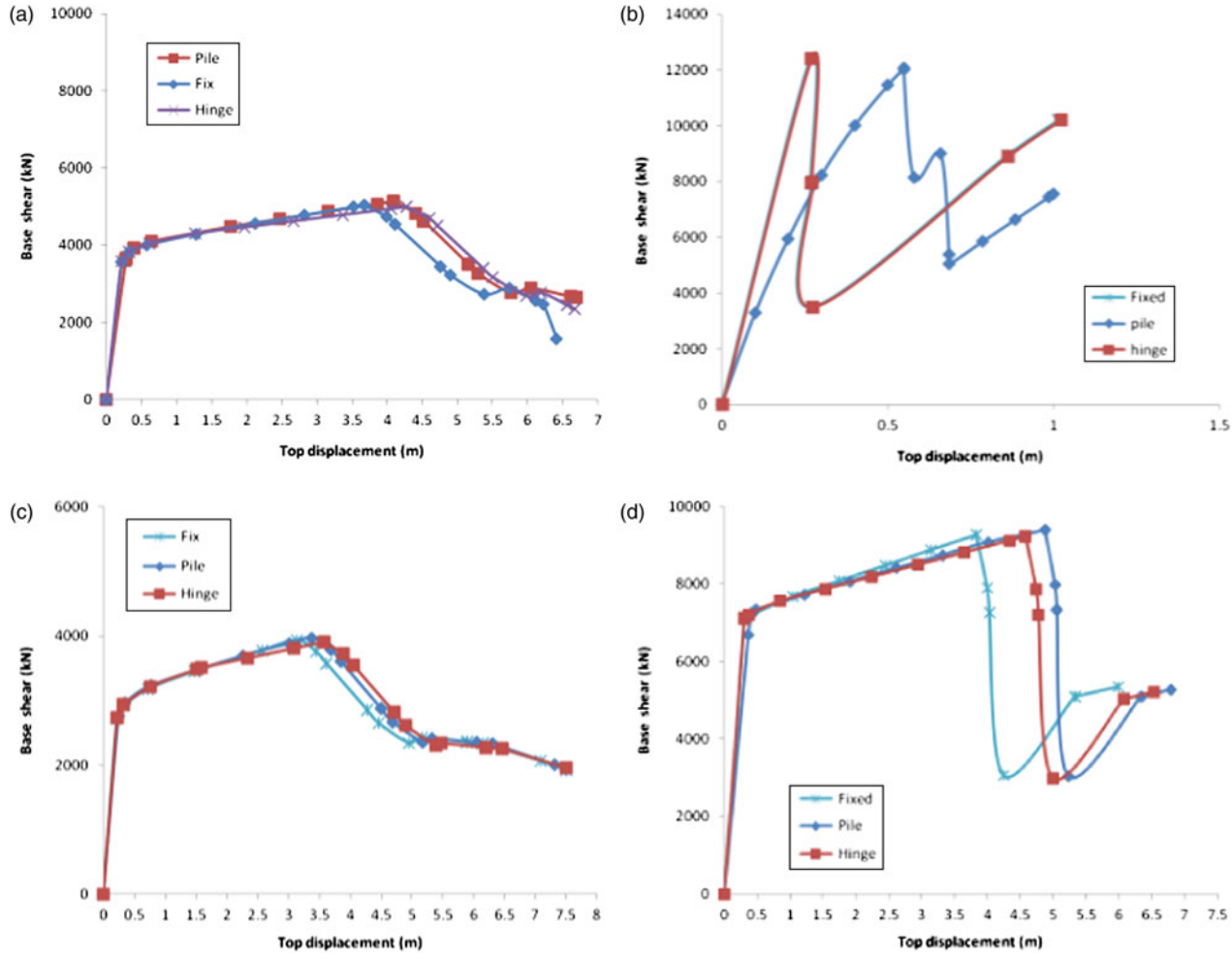

Figure 11. Pushover curves for the models having different end conditions: (a) PD–BRB; (b) FB-Conv; (c) FB–BRB; (d) DBD–BRB.

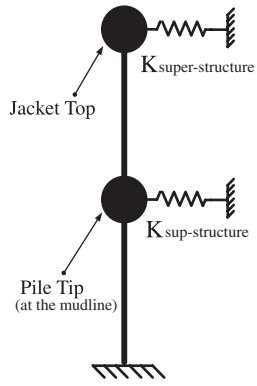

Figure 12. Simplified schematic model for the jacket and the pile–soil system.

4.5 Time-history analysis results

In this section, nonlinear dynamic time-history (NLTH) analyses were carried out using the program code SAP2000 (2005). Kinematic hardening characteristics were considered in the modelling of the force–deformation response of BRB. A frame element with lumped plasticity at both ends is chosen from the SAP2000 library to model the nonlinear behaviour of the structural members. Figure 14 illustrates the hysteretic behaviour and the backbone curve of a BRB applied in the first story of the FB–BRB model. The modal damping ratio of 5% of critical damping is generally used in the analysis of offshore structures (API RP-2A, 2000), which includes the effect of the water–structure interaction and the foundation and structure-related energy dissipation effects.

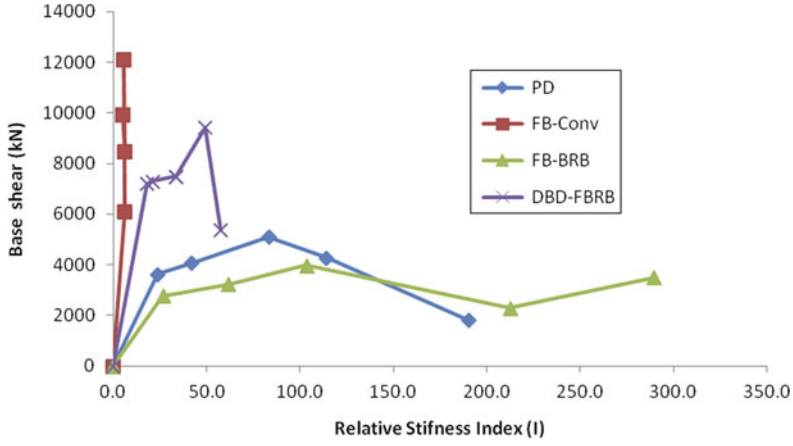

Figure 13. Relation between base shear and the relative stiffness index of the different models.

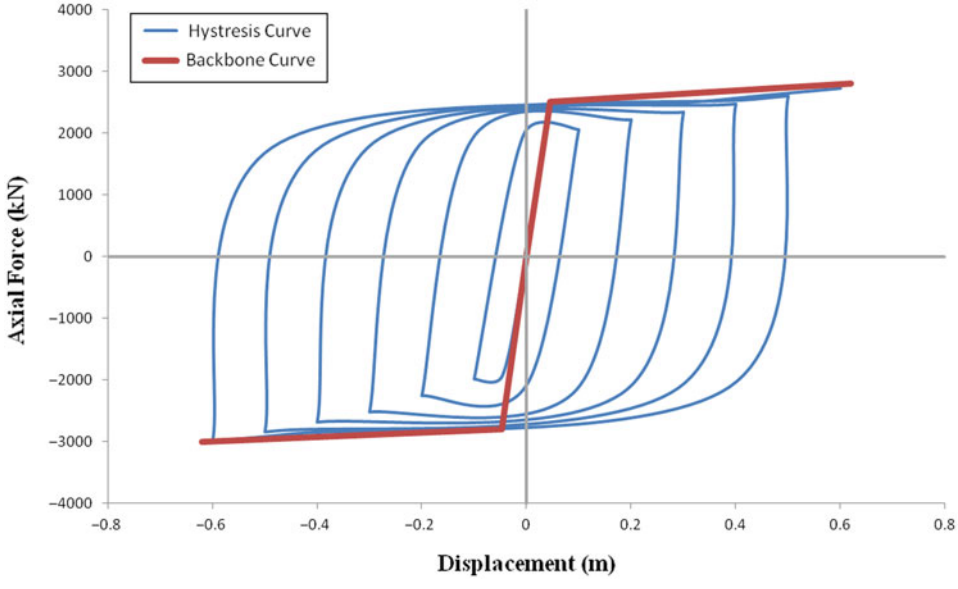

Figure 14. Hysteresis and backbone curves of a BRB in the first story of the FB–BRB model (area $= 50.9\,\text{cm}^2$).

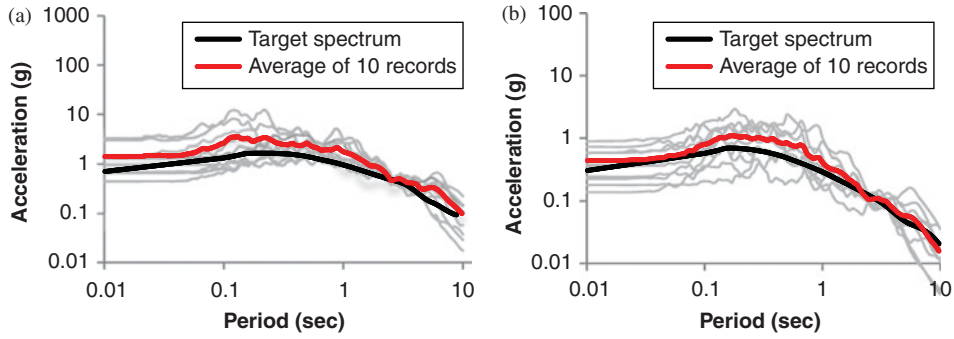

Figure 15. Response spectra of the ground motions and their geometric mean with the target spectra for two-level earthquakes: (a) DLE; (b) SLE.

The seismic performance of the model structures were investigated using ground motion records scaled to the SLE and the DLE hazard-level earthquakes. Two suites of ground motion records scaled to the two hazard levels were selected from the Pacific Earthquake Engineering Research Center (PEER) ground motion database (PEER, 2013) for the NLTH analyses. The ground motion records were scaled in such a way that the geometric mean of the response spectra of each suit of records matches the uniform hazard spectrum with 25% (SLE) and 2% (DLE) probability of exceedance in 50 years in the platform site. The magnitudes of the selected records range from 7.1 to 7.6 with the closest distances to the normal fault varying from 50 to 100 km. All the records were obtained based on the fault–normal orientation and the strike slip condition. Table 5 shows the characteristics of the ground motion suites used in the present study, and Figure 15 shows the response spectra of the ground motions and their geometric mean with the target spectrum.

In this study, the seismic performance of the model structures was evaluated statistically based on the mean and the standard deviation of the MIDR and MTD (maximum top-story drift) values obtained through time-history analyses using the selected ground motion records. MTD and MIDR are generally considered as appropriate engineering demand parameter for offshore platform structures. In such structures, MTD should be maintained within appropriate limits to save the topside equipments which are very important and expensive in comparison with the jacket structure. On the other hand, MIDR accounts for brace buckling which is important for the jacket stability. In addition, monitoring both MTD and MIDR is important for platform conductors which are essential for the function and operation of the whole platform.

By inspecting Table 9, it can be observed that the BRB models generally have much less displacement responses for the DLEs compared with the code-based designed model with conventional braces (FB-Conv). This is attributed to the more uniform pattern of damage distributed throughout the stories of the BRB models. The analysis results for the strength-based earthquakes depicted show that the BRB models generally have larger MTD compared with the FB-Conv case due to their smaller initial stiffness. The DBD–BRB model showed smallest MIDR contributed from the design philosophy considering a desired displacement pattern.

Table 9 presents the mean and standard deviation (SD) of the MTD and MIDR for the different structural models. The mean MTD for the ductility-level ground motions turned out to be the largest in the FB-Conv, which is 44.55 cm, whereas the lowest value occurred in the FB–BRB, which is 22.74 cm. The SD for the FB–BRB is the lowest value of 9.97 cm, and is the largest of 18.2 cm in the PD–BRB. The dispersion in the MTD values is somewhat high in the performance-based designed models compared with the force-based ones.

For the strength-level ground motions, there is a slight difference in values for both the mean and SD among all

Table 9. Maximum response of structural models.

	FB–BRB		PD–BRB		DBD–BRB		FB-Conv.	
	MTD (cm)	MIDR%	MTD (cm)	MIDR%	MTD (cm)	MIDR%	MTD (cm)	MIDR%
Mean								
DLE	22.74	0.57	25.48	0.52	38.69	0.70	44.55	0.75
SLE	21.21	0.50	19.71	0.38	18.26	0.32	17.11	0.39
SD								
DLE	9.97	0.11	18.20	0.26	15.11	0.28	11.71	0.09
SLE	5.43	0.12	6.83	0.09	3.44	0.10	6.78	0.08

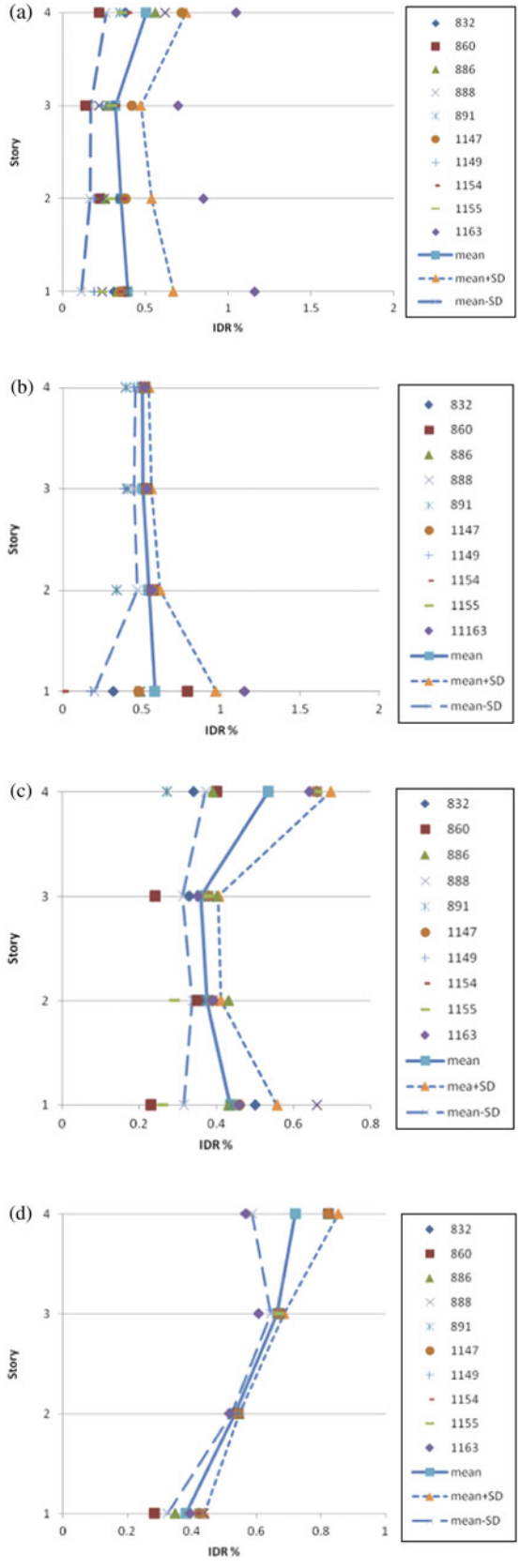

Figure 16. IDRs for DLEs: (a) PD–BRB; (b) DBD–BRB; (c) FB–BRB; (d) FB-Conv.

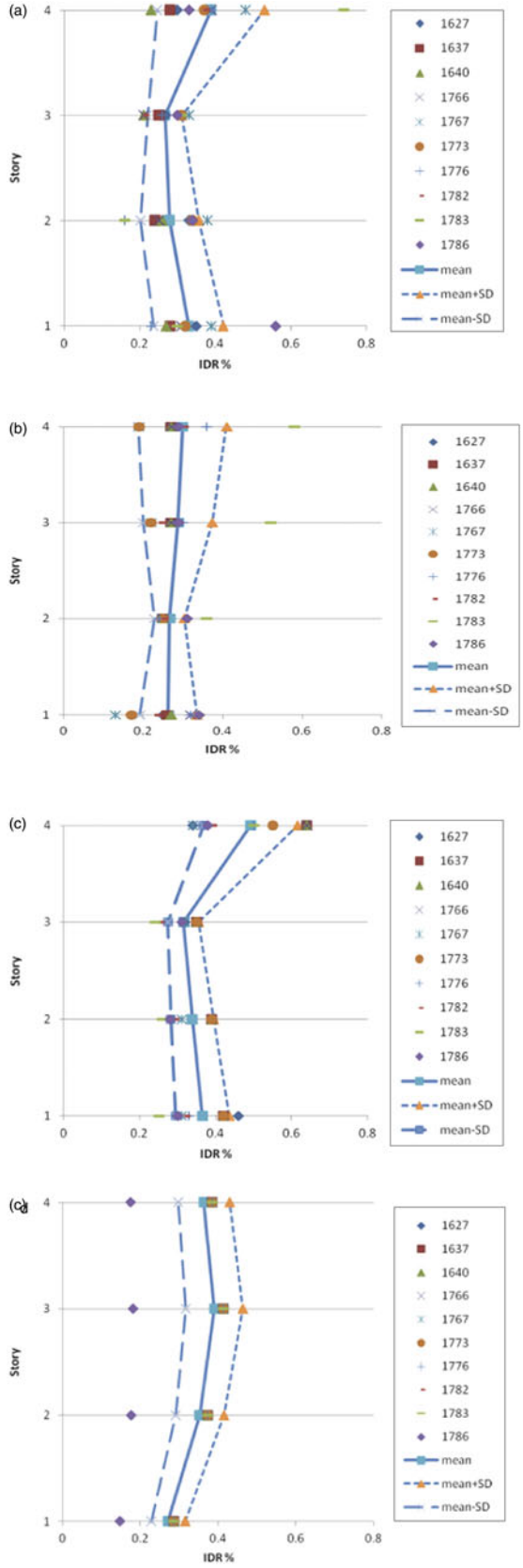

Figure 17. IDRs for SLEs: (a) PD–BRB; (b) DBD–BRB; (c) FB–BRB; (d) FB-Conv.

cases. The mean value of the MIDR for ductility-level ground motions turned out to be the largest in the FB-Conv, which is 1.2%, whereas it is the lowest in the PD–BRB, 0.52%. For strength-level ground motions, all BRB models have similar SD values, whereas the FB-Conv has slightly higher value. Based on the above observation, it can be concluded that the BRB models showed lower seismic displacement responses for ductility-level ground motions compared with the code-designed model with conventional braces.

Figure 16 illustrates the IDR of the model structures subjected to the ductility-level ground motions. It can be observed that the BRB models have a more uniform IDR distribution pattern compared with the FB-Conv, especially the DBD–BRB model. Furthermore, the occurrence of a local failure mechanism in the FB-Conv can be expected from the large IDR value shown at the corresponding story level. It is also observed that the IDR mean values of all model structures, even under the DLE-level ground motions, did not reach the target IDR of 1.75%. For the BRB models, the IDR results from the DLE-level ground motions were well below the target IDR, and the current BRB model design procedures, whether performance- or force-based, may be considered somewhat conservative. In the FB-Conv, however, the upper statistical limit of the MIDR, mean + SD which is 1.5%, found to be close to the target MIDR of 1.75%. For strength-level ground motions, it can be observed that all models have a similar distribution of IDR over the height of the structures as shown in Figure 17.

5. Conclusions

In this study, a pile-founded jacket offshore structure was designed using BRB and conventional braces, and their seismic performances for SLEs and DLEs were compared. The model structures were designed according to three different seismic design methodologies such as the performance-based plastic design, the direct-displacement design method and the force-based design method. The effect of the soil–pile interaction on the global responses was investigated and a relative stiffness index was introduced. Based on the nonlinear static and dynamic analyses, the following findings were derived:

- The model structures designed with BRB showed lower stiffness and strength but larger ductility compared with the structure with conventional bracing.
- The response modification factors of the BRB models obtained from the pushover analysis ranged from about 9 to 22, which is significantly higher than the code-specified values normally used for seismic design of such structures.
- According to nonlinear static and dynamic analysis results, the application of BRB in chevron-braced jacket structures was found to enhance the seismic behaviour under DLEs. However, under SLE, for which the structure behaved almost elastically, the enhancement in seismic capacity was marginal.
- Among the different BRB design methods introduced, displacement-based design method was found to give more uniform plastic hinge distribution, while other methods produced better results in terms of maximum drift ratios. The results showed that a more uniform design lateral load pattern results in uniformly distributed plasticity through the jacket at the intended drift level.
- Based on the relative stiffness index and soil condition introduced in the current study, it was found that for system with large ductility, such as the system with BRB, simplified modelling for soil–pile interaction may be used, especially in the preliminary design stage.
- Based on the amount of steel required for each design method, the performance-based design procedure provided an economic design for pile-founded jacket offshore structures compared with the force-based approach commonly used in the offshore industry.

Funding

This work was supported by Architecture & Urban Development Research Program funded by Ministry of Land, Infrastructure and Transport of Korean government [grant number 13AUDP-B066083-01], and by the Department of Offshore Engineering, Samsung Engineering Co. Ltd.

Note

1. Email: m.nour20@gmail.com

References

American Institute of Steel Construction-341 (2005). *Seismic provisions for structural steel buildings, ANSI/AISC 341-05*. Chicago, IL: Author.

American Institute of Steel Construction-360 (2005). *Specifications for structural steel buildings, ANSI/AISC 360-05*. Chicago, IL: Author.

Anagnostopoulos, S.A. (1983). Pile foundation modeling for inelastic earthquake analyses of large structures. *Engineering Structures*, *5*, 215–222.

American Petroleum Institute (2000). *Recommended practice for planning, design and constructing fixed offshore platforms, API RP-2A* (21st ed.). Washington, DC: Author.

American Society for Civil Engineers-7 (2005). *Minimum design loads for buildings and other structures*. Reston, VA: Author.

Applied Technology Council-19 (1995). *Structural response modification factors*. Redwood City, CA: Author.

Black, C., Makris, N., & Aiken, I. (2004). Component testing, seismic evaluation and characterization of buckling-restrained braces. *Journal of Structural Engineering*, *130*, 880–894.

Building Seismic Safety Council (2004). *NEHRP recommended provisions for seismic regulations for new buildings and*

other structures. Part 1: Provisions, FEMA-450. Washington, DC: Author.

Carden, L., Itani, Buckle, I., & Aiken, I. (2004). *Buckling-restrained braces for ductile end cross frames in steel plate girder bridges*. Proceedings of 13th World Conference on Earthquake Engineering, Vancouver, Canada.

Chao, S.-H., & Goel, S.C. (2005). Performance-based seismic design of EBF using target drift and yield mechanism as performance criteria (Report No. UMCEE 05-05). Ann Arbor, MI: Department of Civil and Environmental Engineering, University of Michigan.

Chao, S.H., & Goel, S.C. (2008). Performance-based plastic design of special truss moment frames. *AISC Engineering Journal*, 2nd Quarter, 127–150. Retrieved from http://wweb.uta.edu/faculty/schao/download/Journal%20Papers/AISC-STMF-PBPD.pdf

Chao, S.H., Goel, S.C., & Lee, S.S. (2007). A seismic design lateral force distribution based on inelastic state of structures. *Earthquake Spectra*, *23*, 547–569.

Coyle, H.M., & Reece, L.C. (1966). Load transfer for axially loaded piles in clay. *Journal of Soil Mechanics ASCE Foundation Division*, *92* (SM2), 1–26.

Fahnestock, L.A., Ricles, J.M., & Sause, R. (2007). Experimental evaluation of a large-scale buckling-restrained braced frame. *Journal of Structural Engineering*, *133*, 1205–1214.

Federal Emergency Management Agency-356 (2000). *Pre-standard and commentary for the seismic rehabilitation of buildings*. Washington, DC: Author.

Goel, S.C., & Chao, S.H. (2008). *Performance-based plastic design earthquake resistant steel structures*. Washington, DC: International Code Council, Washington DC Governmental Affairs Office.

Kiggins, S., & Uang, C.-M. (2006). Reducing residual drift of buckling-restrained braced frames as a dual system. *Engineering Structures*, *28*, 1525–1532.

Kim, J.K., & Choi, H.H. (2004). Behavior and design of structures with buckling-restraint braces. *Engineering Structures*, *26*, 693–706.

Kim, J., Park, J., Shin, S., & Min, K. (2009). Seismic performance of tubular structures with buckling restrained braces. *Structural Design of Tall and Special Buildings*, *18*, 351–370.

Kim, J., & Seo, Y. (2004). Seismic design of low-rise steel frames with buckling-restrained braces. *Engineering Structures*, *26*, 543–551.

Matlock, H. (1970). *Correlations for design of laterally loaded piles in soft clay.* Proceedings of Offshore Technology Conference, Richardson, Houston, TX, USA (pp. 577–594).

Newmark, N.M., & Hall, W.J. (1982). *Earthquake spectra and design*. Oakland, CA: Earthquake Engineering Research Institute.

Osteraas, J.D. (1990). *Strength and ductility considerations in seismic design*. (Doctoral dissertation, Stanford University, Stanford, CA).

Pacific Earthquake Engineering Research Center (2013). *Strong motion data base*. Berkeley, CA: Author.

Priestley, M.J.N. (2000). *Performance-based seismic design*. Keynote Lecture. Proceedings of 12th World Conference on Earthquake Engineering, Auckland, New Zealand.

Priestley, M.J.N., Calvi, G.M., & Kowalsky, M.J. (2007). *Displacement based seismic design of structures*. Pavia: Eucentre Foundation – European Center for Training and Research in Earthquake Engineering.

PTTEP International (2010). Provision of earthquake specific engineering services (site study) for Myanmar Engineering Zawtika Project, Geotechnical Earthquake Engineering Addendum, Doc. No. 09-214-H4.

Rodrigues, P.F.N., & Jacob, B.P. (2005). Collapse analysis of steel jacket structures for offshore oil exploitation. *Journal of Constructional Steel Research*, *61*, 1147–1171.

Sabelli, R. (2000). *Research on improving the design and analysis of earthquake resistant steel braced frames* (Final report). NEHRP Fellowship in Earthquake Hazard Reduction.

Sabellia, R., Mahin, S., & Chang, C. (2003). Seismic demands on steel braced frame buildings with buckling-restrained braces. *Engineering Structures*, *25*, 655–666.

Sahoo, D.R., & Chao, S.H. (2010). Performance-based plastic design method for buckling-restrained braced frames. *Engineering Structures*, *32*, 2950–2958.

SAP2000 (2005). *Structural analysis program, Version 10 – Analysis reference manual*. Walnut Creek, CA: Computers and Structures Inc.

SEAOC (1999). *Blue Book: Seismic design recommendations*. Sacramento, CA: International Code Council.

Tang, X., & Goel, S. (1988). *A fracture criterion for tubular bracing members and its application to inelastic dynamic analysis of braced steel structures*. Proceedings of 9th WCEE, Tokyo, Japan (pp. 285–290).

Uang, C.M., Nakashima, M., & Tsai, K.C. (2004). Research and application of buckling restrained braced frames. *International Journal of Steel Structures*, *4*, 301–313.

Yin, Z., Wang, X., & Li, X. (2009). Hysteretic response and energy dissipation of double-tube buckling restrained braces with contact ring. *Computational Structural Engineering*, 173–179. Retrieved from http://link.springer.com/chapter/10.1007%2F978-90-481-2822-8_20#page-1